WILEY

A Virtual Event Designed For The Masses

Now Available On-Demand!

Scale up your research and translate your results more rapidly and simply than ever before. Welcome to vLC-MS.com - the event for Orbitrap Exploris mass spectrometers and much more!

Tune in to:

- Explore the LC-MS portfolio and meet the expanded Orbitrap Exploris MS system in our staffed Exhibit Hall.
- Learn from mass spectrometry experts, such as Professor Alexander Makarov himself, about Orbitrap mass spectrometry technology and the applications it enables.
- Browse posters and short presentations in our application area.

Event Highlights:

Prof. Alexander Makarov

Dr. Christian Münch

Thomas Moehring

vLC-MS.com

REGISTER NOW

ThermoFisher SCIENTIFIC

Received: 12 June 2019 | Revised: 17 December 2019 | Accepted: 21 December 2019

DOI: 10.1002/pro.3812

THE PROTEIN SOCIETY WILEY

ARTICLE

Solution structure of the nucleotide hydrolase BlsM: Implication of its substrate specificity

Minhee Kang | Kiran Doddapaneni | Samantha Sarni | Zach Heppner | Vicki Wysocki | Zhengrong Wu

Chemistry and Biochemistry Department, Ohio State University, Columbus, Ohio

Correspondence
Zhengrong Wu, Chemistry and Biochemistry Department, Ohio State University, Columbus, OH 43210.
Email: wu.473@osu.edu

Funding information
National Institutes of Health, Grant/Award Number: R21ES024585

Abstract

Biosynthesis of the peptidyl nucleoside antifungal agent blasticidin S in *Streptomyces griseochromogenes* requires the hydrolytic function of a nucleotide hydrolase, BlsM, to excise the free cytosine from the 5′-monophosphate cytosine nucleotide. In addition to its hydrolytic activity, interestingly, BlsM has also been shown to possess a novel cytidine deaminase activity, converting cytidine, and deoxycytidine to uridine and deoxyuridine. To gain insight into the substrate specificity of BlsM and the mechanism by which it performs these dual function, the solution structure of BlsM was determined by multidimensional nuclear magnetic resonance approaches. BlsM displays a nucleoside deoxyribosyltransferase-like dimeric topology, with each monomer consisting of a five-stranded β-sheet that is sandwiched by five α-helixes. Compared with the purine nucleotide hydrolase RCL, each monomer of BlsM has a smaller active site pocket, enclosed by a group of conserved hydrophobic residues from both monomers. The smaller size of active site is consistent with its substrate specificity for a pyrimidine, whereas a much more open active site, as in RCL might be required to accommodate a larger purine ring. In addition, BlsM confers its substrate specificity for a ribosyl-nucleotide through a key residue, Phe19. When mutated to a tyrosine, F19Y reverses its substrate preference. While significantly impaired in its hydrolytic capability, F19Y exhibited a pronounced deaminase activity on CMP, presumably due to an altered substrate orientation as a result of a steric clash between the 2′-hydroxyl of CMP and the ζ-OH group of F19Y. Finally, Glu105 appears to be critical for the dual function of BlsM.

KEYWORDS

BlsM, nucleotide hydrolase, NMR structure, enzyme mechanism, N-glycosidase

1 | INTRODUCTION

Biosynthesis of the antifungal agent blasticidin S in *Streptomyces griseochromogenes* depends on the function of BlsM, a member of a new family of hydrolases. Because the intracellular free cytosine concentration is low, BlsM

ABBREVIATIONS: CMP, cytidine monophosphate; dCMP, deoxycytidine monophosphate; hmCMP, hydroxylmethyl CMP; HSQC, heteronuclear single quantum coherence; NDT, nucleoside deoxyribosyltransferase; NMR, nuclear magnetic resonance; TROSY, transverse relaxation optimized spectroscopy.

is critical for releasing free cytosine by specifically catalyzing the hydrolysis of the N-glycosidic bond of CMP or dCMP.[1] MilB and RCL are two other known members of this hydrolase family. MilB is responsible for the liberation of hydroxyl methyl CMP in biosynthesis of mildiomycin,[2] and RCL, one of the most responsive genes to c-myc during tumorigenesis, specifically cleaves the glycosidic bond in dGMP.[3] Although, these hydrolases are functionally similar to the nucleoside hydrolases (NHs) that were initially identified and characterized as nucleoside salvage enzymes in parasitic protozoa,[4,5] sequence alignment has suggested structural and mechanistic similarity with the family of 2′-deoxyribosyltransferases (DRTases).[6] DRTases have also been identified in parasites, however, no homologous enzyme has been identified in mammals.[7] DRTases cleave the N-glycosidic bond of a nucleoside through formation of a covalent enzyme-deoxyribose intermediate, followed by a reverse reaction between the original sugar and a nucleobase.[8] BlsM, MilB, and RCL differ from DRTases by lacking the transferase activity despite that RCL can form a similar covalent enzyme-substrate intermediate during hydrolysis reaction.[9] Finally, these hydrolases specifically hydrolyze a nucleotide whereas DRTases preferentially recognize a nucleoside.

The structure of RCL has been determined previously,[10,11] showing several polar residues residing within the active site pocket. Among them, Glu93 and Ser87 are conserved in all members in this hydrolase family. Kinetic studies later revealed that the glutamate serves as a nucleophile to form the covalent enzyme-substrate intermediate, while the serine is one of the key residues for recognizing the 5′-phosphate group of dGMP.[9] In addition, it was also revealed that both Ser117 and Tyr13 are important for the activity of RCL and are conserved in all RCLs from different species. The side chain of Ser117 protrudes into the active side pocket of the neighboring monomer. Together with Ser87, they form a phosphate group binding site near the dimer interface. Tyr13 plays a critical role during the chemical cleavage of the glycosidic bond. The counterpart of Tyr13 in NDT, a member of DRTase family, has been suggested to help orient either the substrate or the nucleophilic glutamate residue.[6] Interestingly, neither of these two catalytically important residues is conserved in BlsM or MilB. Recent structural studies on MilB indicated that a phenylalanine in place of the tyrosine at the equivalent position changed its substrate preference.[12] Furthermore, these hydrolases differ from DRTases by having rather rigid substrate specificity. RCL has a high preference for dGMP as a substrate, whereas its hydrolytic activity on GMP is several orders of magnitude lower.[9] BlsM prefers CMP over dCMP slightly, and MilB prefers hydroxylmethyl CMP (hmCMP).[7] Further, BlsM uniquely possesses a weak cytidine or deoxycytidine deaminase activity.[1] This result is quite intriguing, as all known cytidine deaminases require a Zn ion for catalysis,[13] however, no members of this hydrolases family retains the conserved metal binding site commonly observed in all deaminases.

In order to understand sequence and structural determinants that confer its sugar and nucleobase specificity and the mechanism by which it performs the dual function, we determined the solution structure of BlsM from *S. griseochromogenes* using multidimensional nuclear magnetic resonance (NMR). BlsM adopts an overall tertiary fold of a home-dimer, similar to both RCL[10,11] and MilB,[12,14] with each monomer consisting of a five-stranded β-sheet that is sandwiched by five α-helices. In comparison to other members in this hydrolase family, the structure provides rationales on the sequence conservation of certain key active site residues and the variations that lead to substrate specificity. Combined with site-directed mutagenesis and steady state kinetic studies, our results confirmed the double displacement mechanism during hydrolysis and also shed light on the mechanism by which BlsM selects between its dual functions, depending on the relative orientation of the enzyme and the substrate.

2 | RESULTS

2.1 | Structural determination

Recombinant WT BlsM and its mutants were overexpressed and purified to homogeneity. All the BlsM variants exhibited similar size-exclusion elution profiles, displaying a mono-dispersive species with an elution volume corresponding to a dimer with an apparent molecular mass of ~37 kDa. This result is consistent with the previous prediction based on protein sequence that BlsM shares a DRTase domain that adopts a dimeric structure as the functional unit.[6] A recent study on a similar nucleotide hydrolase, RCL, also showed that the dimeric arrangement is critical for its enzymatic activity.[9] The solution structure of the WT BlsM has been determined using multidimensional NMR. Figure 1 shows the 2D ^{1}H-^{15}N TROSY spectrum of BlsM exhibiting well-dispersed resonances. Ninety-three percent of non-Pro residues in the native sequence have been assigned using TROSY-based triple resonance experiments. The residues with vanishingly weak amide signals include Leu20, Phe24, Met25, Phe58-Ala60, and Arg62-Glu64 from the two internal loops (Loop I and Loop II), Phe130 near the domain interface and Asp148 located in the turn between

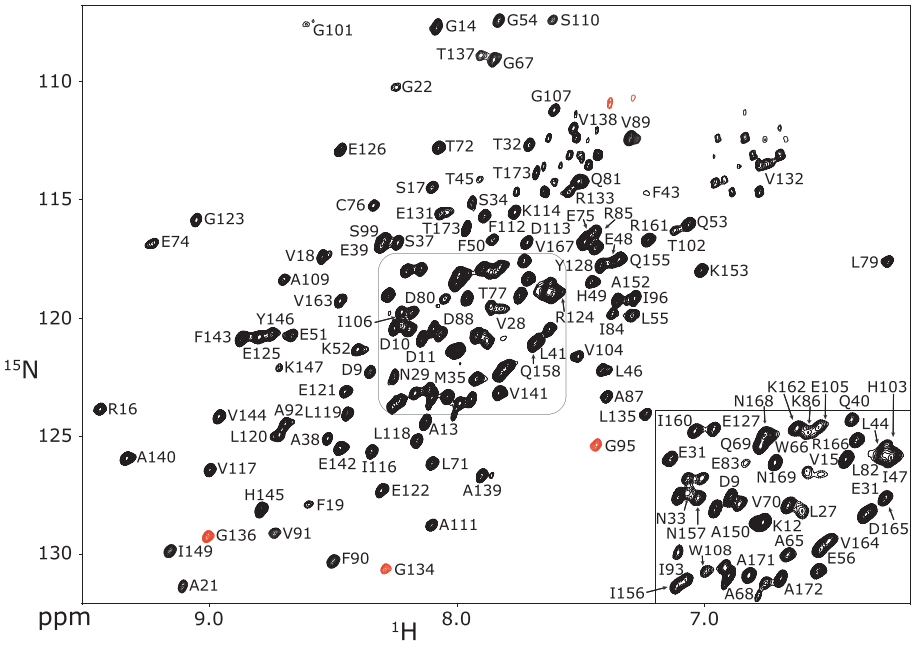

FIGURE 1 2D ^{1}H-^{15}N TROSY of BlsM labeled with one latter code and residue number. Peaks in the boxed region are labeled in the insert. The three glycine resonances in red, Gly95, Gly136, and Gly134 are aliased from the top of the spectrum

the last β-strand and the last α-helix, likely due to either fast exchange with solvent or conformational exchange on an intermediate NMR timescale. The ensemble structures were calculated using a total of 1,682 experimentally determined restraints per monomer, including 106 intermolecular distance restraints, 272 backbone dihedral angles and 86 unambiguous residual dipolar couplings (RDC), as summarized in Table 1. Figure 2a shows the superposition of 15 lowest energy structures with a backbone RMSD value of 0.39 or 0.45 Å for the monomer or dimer, respectively, based on the backbone atoms within the structured regions. PROCHECK analysis indicated that ~99.3% of the residues are within the allowed region of the Ramachandran plot, with only one exception, Phe130, which, as will be discussed later, is located near the domain interface, engaging in extensive hydrophobic interaction with residues from the neighboring monomer.

TABLE 1 NMR structural statistics of BlsM

Total constraints	1,682
Long range NOE ($5 \leq i - j$)	648
Short range NOE ($1 \leq i - j < 5$)	570
Intermolecular NOE	106
Dihedral angle restraints ϕ and φ	272
RDC in 12 mg/mL Pf1 phage	86
Structure statistics (15 structures)	
Violation statistics	
Distance constraints (Å)	0.036 ± 0.003
Maximum distance violation (Å)	0.5
Deviations from idealized covalent geometry	
Bond lengths (Å)	0.00267 ± 0.0002
Bond angles (°)	0.521 ± 0.030
PROCHECK (Ramachandran plot)	
Most favored region (%)	77.2
Generously allowed region (%)	22.1
Disallowed region (%)	0.7
RMSDs from the average structure (Å)	
Backbone atoms: monomer (dimer)	0.39 (0.45)

2.2 | BlsM structure

BlsM exists in solution as a symmetric dimer, with each monomer consisting of a five-stranded parallel β-sheet that is sandwiched between five α-helices, resembling a conventional Rossmann fold (Figure 2b). The five β-strands arrange in an order of 2, 1, 3, 4, and 5. The structure fold starts from the β1 (Ser17-Gly22), which is flanked by β2 (Glu56-Asn59) and β3 (Val89-Pro94). β4 (Ile116-Ile120) lies parallel next to the β3, and the β5 (Ala140-Tyr146) in turn next to β4 completing the β-sheet. Two α-helices, α1 (Ala38-Lys52) and α5 (Ala152-Arg166), interact with one side of the β-sheet, while the other three α-helices, α2 (Pro73-Lys86), α3 (Pro100-Ala111), and α4 (Pro115-Ile120) are located on the other side. These three α-helices simultaneously make extensive contacts with the same α-helices, α2′, α3′, and α4′ (“” denotes residues and secondary elements from

the neighboring monomer hereafter). Intermolecular interactions are mediated through hydrophobic side-chains, including Thr77, Pro78, Leu82, His103, Val104, Trp108, Ala111, Phe112, Phe130, Ile131, and Val138, as exemplified by the methyl group of Ala111 from α3 (Figure 3). Specifically, Ala111 not only makes unambiguous NOE contacts with the aromatic rings of Trp108', Phe112', but also with its symmetric counterpart (Ala111') across the domain interface. It is noteworthy that intramolecular NOE crosspeaks are effectively suppressed as evidenced by the complete removal of Val89-CH_3 spin system and the strong intra-residue methyl-to-amide cross peak (Figure 3a). Additional intermolecular contacts are also observed for several residues, namely Val28 and Val70, located in Loop I and Loop II. Three glycine residues, Gly101 and Gly107 from α3 and Gly134 from α4, are located at the center of these two interfacial α-helices, presumably allowing close intermolecular interaction between the two monomers. These three glycine residues are conserved in all DRTase-like proteins, suggesting that a dimeric topology is an important common feature shared by all of those enzymes.

2.3 | BlsM active site

Previously, two residues, Glu105 and Ser89, have been demonstrated to be catalytically important.[1] Our structure

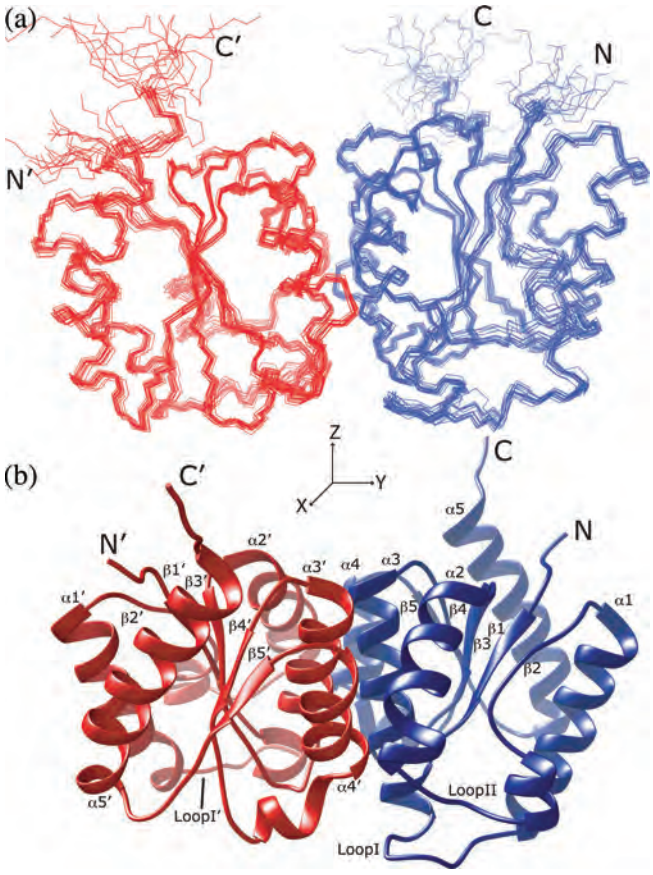

FIGURE 2 (a) Superposition of 15 lowest energy structures of BlsM generated by NOE-derived distance restraints, backbone torsion angles, and residual dipolar couplings; (b) Ribbon representation of BlsM dimer, with the two monomers being colored in red and blue. The N- and C-termini of the two monomers are labeled as N and C, and N′ and C′, respectively

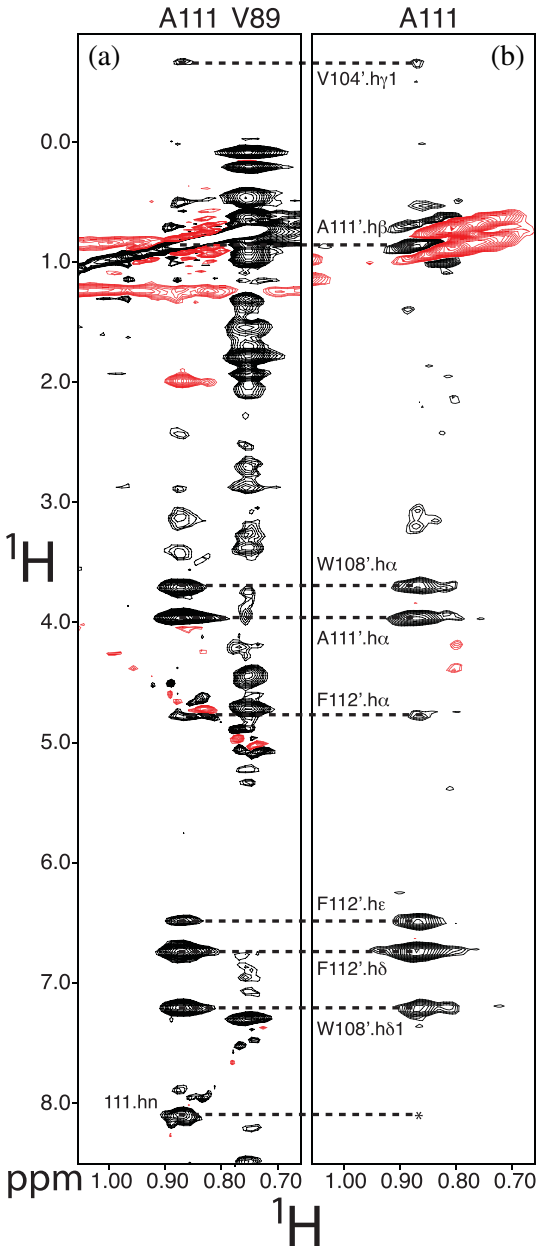

FIGURE 3 Strips of (a) 3D ^{13}C-edited and (b) ^{13}C-filtered ^{13}C-detected NOESY spectra for Ala111 β-CH_3, showing the intermolecular contacts with Val104', Ala111', Phe112', and Trp108'. Complete suppression of intramolecular NOEs is evidenced by missing strong intra-residue NOE cross peak to its own amide proton (noted by asterisk in the filtered data) and the entire Val89 methyl system observed in (a)

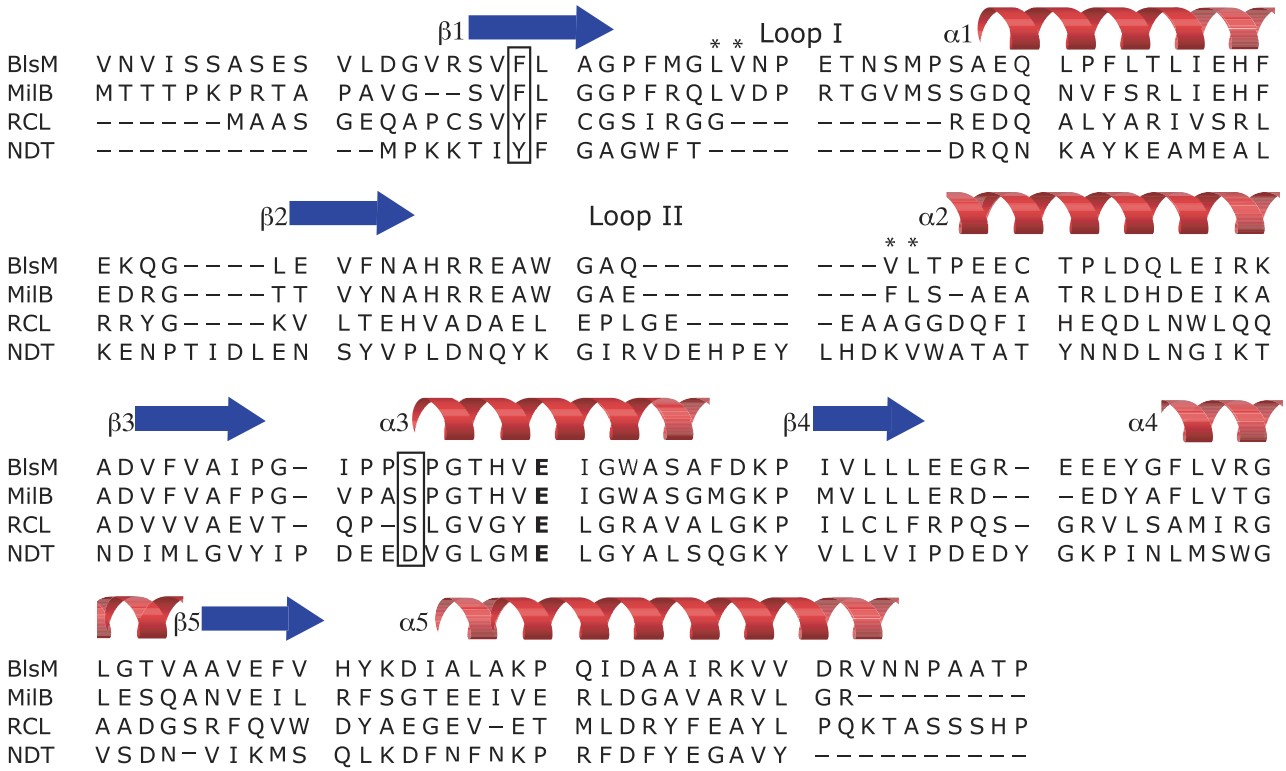

FIGURE 4 Sequence alignment of BlsM from *Streptomyces griseochromogenes*, MilB from *Streptomyces rimofaciens*, RCL from *Rattus norvegicus*, and NDT from *Lactobacillus leichmannii*. The conserved nucleophilic glutamate residue is in bold, and the key residues responsible for discriminating nucleotide vs. nucleoside or selecting ribose against deoxy-ribose are boxed, and the large hydrophobic residues in Loop I and II are noted with asterisk

revealed that both of these two residues are located within a pocket, encircled by the β1, β2, α2, α3, and the Loop I and II. Compared with the structures of RCL[10] and MilB,[12,14] Glu105 and Ser89 coincide, respectively, with the counterpart active site residues Glu93 and Ser87 in RCL and Glu103 and Ser97 in MilB, suggesting a similar catalytic role for Glu105 as a nucleophile and Ser89 as a critical residue for 5′-phosphate group recognition.[9] In addition, the side chains of Phe24 and Met25 project into the active site pocket, consistent with the previous structural study results of MilB that Phe24 stabilizes the pyrimidine ring of the hmCMP substrate, while Met25 plays an important role in selection for CMP against hmCMP.[14]

Sequence alignment of BlsM with RCL,[10] MilB,[12,14] and *Lactobacillus Leichmanni* nucleoside deoxyribosyltransferase (NDT)[6] (Figure 4) revealed that both BlsM and MilB have a longer Loop I and a shorter Loop II, each of which contains two large hydrophobic residues. Our structure shows that the side chains of Val70 and Leu71 from Loop II reside close to the domain interface, making hydrophobic contacts with the side chains of Leu27 and Val28 from Loop I. Phe130′ from the neighboring monomer protrudes its aromatic side chain into this cluster of hydrophobic network, closing off the active site pocket near the domain interface (Figure 5a). As a result, all catalytically important residues in each active site of BlsM are exclusively from one monomer. RCL and NDT, on the contrary, lack of similar hydrophobic residues within Loop I and II (Figure 5b). Therefore, their catalytic pockets are comparatively more open toward the domain interface, allowing the participation of an important polar residue from the neighboring monomer for substrate binding.[6,10,11] For example, Ser117′ from RCL is a highly conserved residue among a variety of species and it is important for recognition of the 5′-phosphate group of dGMP.[10] In BlsM, this serine residue is replaced by a glycine (Gly129′), which is rotated away from the domain interface, allowing the aromatic ring of Phe130′ to make the hydrophobic contacts mentioned above. Consistently, the X-ray crystal structure of the homologous hydrolase, MilB, also shows no direct participation by the adjacent protomer in binding a sulfate ion.[12]

2.4 | BlsM catalyzes the hydrolysis of CMP through an enzyme-substrate covalent intermediate

It has been shown that the homologous hydrolase RCL catalyzes the hydrolysis of dGMP using a ping-pong

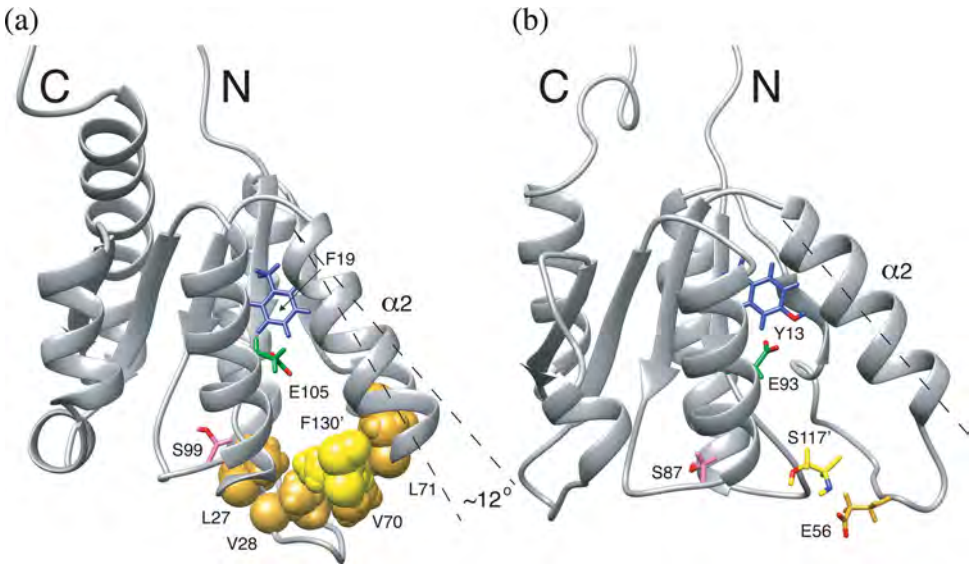

FIGURE 5 Comparison of the active site pockets of BlsM (a) and RCL (b). The orientation of BlsM is 90° rotated along the *z*-axis from Figure 2b. One monomer is shown for each protein, viewing into the active site pocket from the domain interface. (a) displays the hydrophobic interaction among the side chains of Leu27, Val28, Val70, and Leu71 from Loop I and Loop II (dark yellow) and that of Phe130′ (light yellow) from the adjacent monomer; and (b) shows the insertion of the polar side chain of Ser117′ of RCL from the neighboring monomer and lack of extensive hydrophobic interaction as seen in BlsM. Dashed lines indicate the relative angle between the helix 2 (α2) of BlsM and RCL

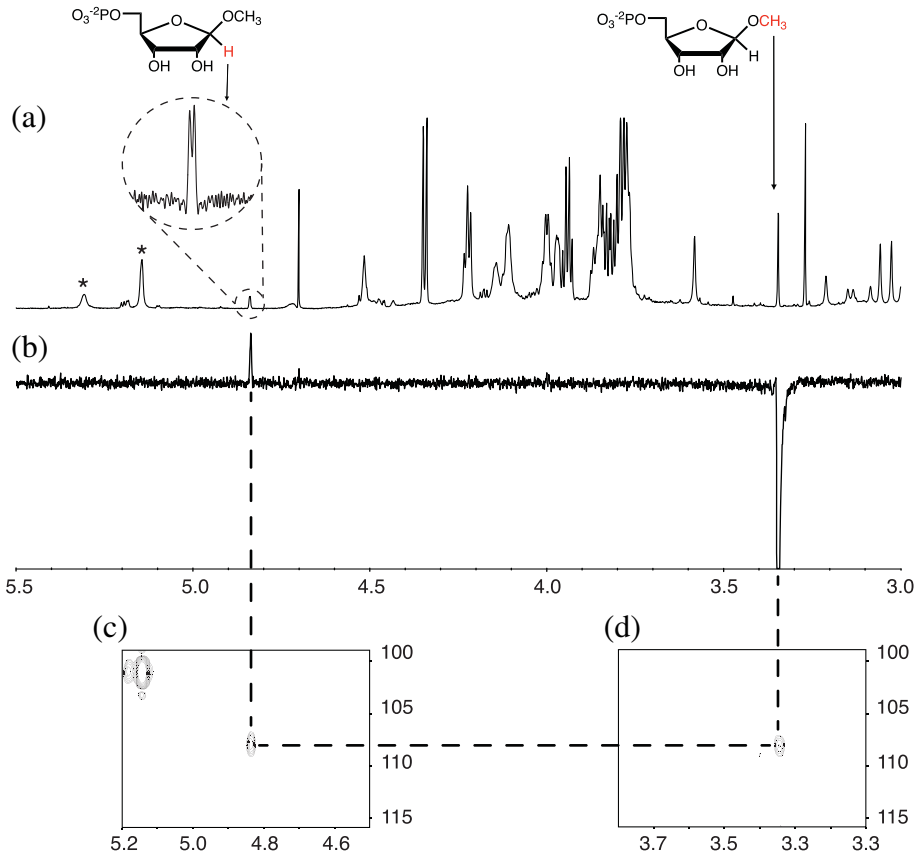

FIGURE 6 NMR studies of methanolysis of CMP by BlsM: (a) ^{1}H spectrum of the hydrolysis mixture of CMP in the presence of 20% methanol; (b) ^{1}H NOESY spectrum when the 3.34 ppm methyl protons were selectively saturated; (c) Selected 2D ^{1}H-^{13}C HSQC showing the H1′–C1′ correlation, and (d) 2D ^{1}H-^{13}C HMBC revealing three-bond *J* correlation between —OCH_3 proton and C1′ carbon. The two resonances denoted by asterisk in (a) correspond to the anomeric H1′ of R5P, as a result of tautomerization. The insert displays the H1′ doublet of the methylated-R5P with the *J*-coupling constant expected for β-configuration

TABLE 2 Kinetic properties for BlsM WT, and its mutants using dCMP and CMP as the substrates

	CMP			dCMP		
Enzyme	k_{cat} ($\times 10^{-2}$ s^{-1})	K_M (μM)	k_{cat}/K_M (M/s)	k_{cat} ($\times 10^{-2}$ s^{-1})	K_M (μM)	k_{cat}/K_M (M/s)
WT	1.15 ± 0.21	35.5 ± 4.1	325 ± 34	0.94 ± 0.05	55.1 ± 19.6	171.9 ± 55.8
F19Y	0.011 ± 0.0004	48.3 ± 9.0	7 ± 0.5	2.23 ± 0.071	51.4 ± 8.4	731.8 ± 83.2
F19A	0.032 ± 0.007	198 ± 60.0		0.32 ± 0.02	89.0 ± 23.1	
F19S	0.014 ± 0.001	82.4 ± 25.7		0.38 ± 0.04	93.4 ± 34.7	

mechanism by first formation of a covalent enzyme-substrate intermediate followed by nucleophilic attack by a solvent molecule. Compared to an alternative mechanism of hydrolysis in which a water molecule may directly attack the substrate, the ping-pong mechanism preserves the β-conformation of the ribose in the final product. To demonstrate BlsM utilizes a similar mechanism, we probed the formation of an enzyme-substrate intermediate by carrying out the hydrolysis reaction in the presence of 20% methanol. The reaction mixtures were subsequently analyzed by NMR, and the results are shown in Figure 6. Two new proton resonances were observed at 4.84 and 3.34 ppm in the presence of methanol, presumably corresponding to the H1′ and the methoxy group, respectively. Their identity was proved by their characteristic directly attached carbon chemical shifts measured by 2D $^{1}H/^{13}C$-HSQC experiment. During the progression of the methanolysis reaction, the intensity of these two signals increased concurrently, with their relative intensity ratio being consistently maintained around 1:3. To confirm that the methoxy group is directly attached to the anomeric carbon of the ribose as the predicted methanolysis product, 1-*O*-methyl-ribose 5′-monophosphate (MeO-R5P), first we performed selective NOE experiment (Figure 6b). Selective saturation of the methyl signal at 3.34 ppm allowed detection of the 4.86 ppm proton signal, indicating the methoxy group is spatially in close proximity to the H1′. Second, we performed 2D ^{1}H-^{13}C HMBC (Figure 6d) to confirm that the methyl protons are scalar-coupled to the C1′ carbon of the ribose at 108.2 ppm. Careful examination of the splitting pattern of the H1′ resonance revealed a ~1.5 Hz J-coupling, which is in good agreement with the reported value of $J_{H1'\text{-}H2'}$ in methyl-β-ribofuranoside but now that of the corresponding α-anomer.[15] Collectively, unambiguous identification of the β-MeO-R5P rules out a mechanism involving direct nucleophilic attack by an enzyme-activated water molecule,[16,17] and strongly suggests that BlsM hydrolyzes CMP via the formation of an intermediate in a manner similar to RCL,[9] the transfererases,[8] and the retaining glycoside hydrolases.[18]

2.5 | Phe19 selects CMP over dCMP

Sequence alignment in Figure 4 revealed that BlsM prefers a phenylalanine residue at the position equivalent to the conserved Tyr13 in RCL. We have previously shown that mutation of Tyr13 in RCL to a phenylalanine significantly reduced its hydrolytic activity on dGMP by ~300-fold.[9] In order to uncover the catalytic role of Phe19 in BlsM, we mutated this residue to a tyrosine, a serine, and an alanine, and performed kinetic analysis of their activity using both ^{32}P-labeled CMP and dCMP; and the results are summarized in Table 2. Consistent with the published results,[1] WT BlsM displayed similar kinetic activities for CMP and dCMP, with a slightly higher preference for CMP. When Phe19 was mutated, the K_m values were virtually unaffected for all three mutants, suggesting that this residue is unlikely to directly participate in substrate binding. However, all three mutants exhibited significant decrease in hydrolytic activity on CMP, with 40- to 100-fold reduction in k_{cat} and ~50-fold reduction in k_{cat}/K_m. Single turnover kinetic assay (not shown) also showed a similar reduction in k_{obs} for CMP, which is as expected of residues that plays critical role during the chemical cleavage of the glycosidic bond, suggesting that Phe19 may participate in a rate-limiting step up to and including the chemical cleavage of CMP. Surprisingly, when dCMP was used as the substrate, the hydrolytic activities of all three mutants were not significantly affected as did for CMP. In fact, F19Y showed a slight increase in k_{cat} and a ~5-fold increase in k_{cat}/K_m with respect to the WT enzyme. Consequently, F19Y displayed a more than 100-fold enhancement on substrate specificity for dCMP over CMP. A similar result was also obtained for MilB, suggesting that a phenylalanine residue is required for effective hydrolysis of CMP and a tyrosine favors dCMP as the substrate.[12] This result is consistent with the fact that both deoxynucleotide hydrolase RCL and deoxynucleoside transferase NDT utilize a tyrosyl residue at this position, as their natural substrates are dGMP and deoxy-nucleoside, respectively. As the conclusion, the type of amino acid at this

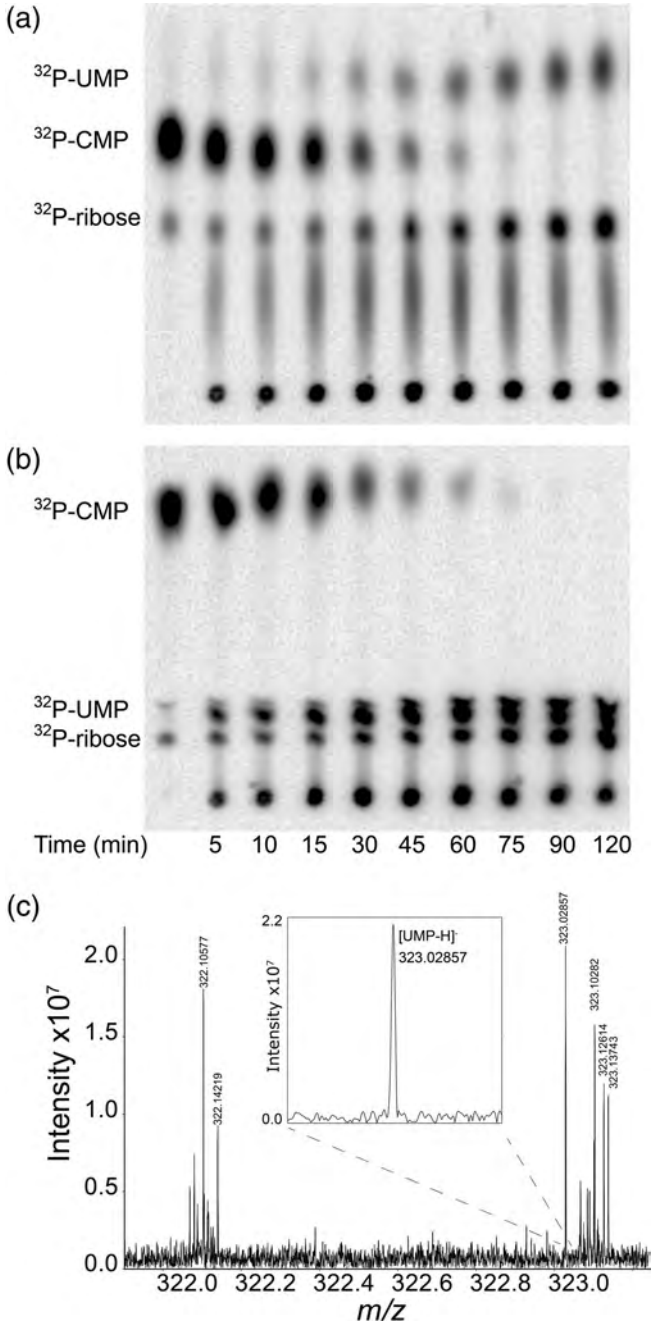

FIGURE 7 Deamination activity of F19Y. Single turn over experiment of F19Y on CMP, analyzed by (a) 0.5 M LiCl; (b) 0.9 M acetic acid + 0.3 M LiCl buffer; (c) Mass-spectrometry analysis of the reaction mixture, with a zoomed in insert demonstrating the presence of UMP. The cluster of peaks located at m/z 322.1 and 323.1 are background peaks. The peak at m/z 323.02857 and its corresponding inset have been identified as UMP ($C_9H_{12}N_2O_9P$) with an error of 0.06 ppm; another possible match to the m/z 323.02857 peak is $C_{12}H_3N_8O_4$ with a larger error of 0.91 ppm.

position dictates the substrate specificity and replacing the phenylalanine with a tyrosine residue reverted the sugar preference of BlsM.

2.6 | F19Y has a pronounced deaminase activity

During the measurement of the hydrolytic activity of F19Y on CMP, we noticed the formation of a new product that did not correspond to ^{31}P-ribose. As shown in Figure 7a, slow hydrolysis of CMP was concurrent with another reaction that produced a compound that migrated faster than the expected product. Since it was previously reported that BlsM has a weak cytidine deaminase activity, capable of converting cytidine and deoxycytidine to uridine and deoxyuridine, respectively,[1] we speculated that this new product is UMP. In order to confirm the nature of this compound, we first analyzed the reaction mixture using a different TLC buffer system (Figure 7b). These two buffer systems were previously used for the detection of deaminase activity of APOBEC1, a well-known cytidine deaminase.[19] As expected, the migration pattern of the reaction mixture of F19Y resembled the published results of the deamination reaction of dCMP by APOBEC1.[19] Next, the reaction mixture was subjected to further analysis by mass-spectrometry, which unambiguously confirmed the presence of UMP in the reaction mixture of F19Y (Figure 7c). It is noteworthy that this deamination activity is insensitive to variable EDTA concentration, suggesting that the deamination capability of F19Y is metal independent. Since all known deaminases possess a catalytic glutamate, we next obtained a double mutant, F19Y/E105A. No detectable amount of UMP was produced within the experimental timeframe, implying that the deaminase activity of BlsM may also utilize a glutamate, Glu105, as one of the active site residues. Thus, BlsM is a dual function enzyme, with its hydrolytic activity being dominant toward its nature substrates, CMP and/or dCMP. When mutated or bound to a noncognate substrate, BlsM may act as a deaminase.

3 | DISCUSSION

3.1 | Structural comparison

The solution structure of BlsM determined by NMR demonstrates a symmetric dimeric arrangement, with each monomer containing a typical α/β Rossman fold. Superposition of our structure with those of MilB (PDB code 4JEL) and RCL (PDB code 2KHZ) resulted the backbone pairwise RMSD values of 0.94 and 1.88 Å, respectively, for 86 aligned backbone atoms. Apparently, the structure of BlsM closely resembles that of MilB, however, it differs from RCL significantly. One of the major differences is the position of helix α2. In BlsM, the C-terminal end of α2 shifts toward α3 by ~12° when compared to the same helix

in RCL (Figure 5). This is likely due to the extensive hydrophobic interaction between the side-chains of Leu27 and Val28 from Loop I and those of Val70 and Leu71 from Loop II. These residues are located opposite to the catalytically important residues Glu105 and Phe19, close to the dimer interface. Together with the side chain of Phe130′, they form a hydrophobic barrier. Sequence alignment of all known BlsM and MilB homologs from different species indicated that hydrophobic amino acids are conservatively preferred at those positions. RCL and NDT, on the other hand, lack of similar hydrophobic residues in Loop I and II. Consequently, the active site pocket of BlsM is comparatively smaller and more enclosed, whereas those of RCL and NDT are more open and extended toward to the domain interface. The open active site pocket of RCL or NDT allows one polar residue from the neighboring monomer, Ser117′ in RCL or Asn123′ in NDT, project its side chain into the active site. Both of these residues have been previously reported to be responsible for facilitating substrate binding.[6,10] This structural difference observed between BlsM and RCL may presumably attribute to their substrate specificity, as a smaller pyrimidine substrate fits a more confined pocket, as in BlsM and MilB, whereas a larger purine nucleobase requires accommodation by a more open active site, as in RCL and NDT.

Functionally, BlsM is quite similar to MilB, except that MilB preferentially hydrolyzes 5-hmCMP.[2] The crystal structure of MilB in complex with its substrate indicates that two residues from Loop I are important for the interaction with the base of hmCMP, one of which is an aromatic amino acid (Phe22) and the other is a positively charged one (Arg23).[14] Phe22 was suggested to make hydrophobic contact with the base, while Arg23 is responsible for differentiating an hmCMP versus a CMP. In BlsM, the equivalent residue to Arg23 is Met25, an un-charged amino acid, which was again suggested by Zhao to help preferentially select CMP. Similar to the structure of apo-MilB, our solution structure of apo-BlsM displays a short α-helix between Phe24-Val28, allowing the side chain of Phe24 and Met25 coincide with their counterpart in apo-MilB. Additionally, the broadening of their backbone amide resonances in 2D-HSQC suggests conformational sampling at an intermediate NMR timescale. This is consistent with the structural results of MilB that Arg23 adopts different conformations in the presence and absence of hmCMP and the short α-helix where Arg23 is located switches to a coiled structure upon binding of the correct substrate, hmCMP, but not upon binding of CMP.[14]

3.2 | Reaction mechanism

Our methanolysis results confirmed the formation of β-MeO-R5P, a product expected for a double displacement mechanism involving a covalent enzyme-sugar intermediate.[17,20] It is noteworthy that the formation of the methanolysis product kinetically parallels with the formation of R5P. It has been previously shown for RCL that the reverse reaction from dR5P to MeO-dR5P can happen, however, at a much slower rate. Significant increase of the methylated product may be observed only with prolonged incubation at the consumption of dR5P after all dGMP substrates were hydrolyzed.[9] During our methanolysis experiment for BlsM, reaction progress was monitored continuously at different time points. The integrated peak intensity of H1′ of R5P and that of OCH_3 from MeO-R5P increased concurrently with their ratio being relatively constant during our experimental period, suggesting formation of R5P and MeO-R5P are two independent and parallel reactions. In conclusion, our methanolysis results are in good agreement with the outcomes expected for a ping-pong mechanism in which a reaction intermediate is first formed, followed by solvent nucleophilic attack.

3.3 | Selection of CMP versus dCMP by Phe19

Our kinetic studies of WT BlsM and the F19Y mutant indicated that Phe19 is important for differentiating a ribonucleotide versus its deoxyribosyl counterpart. Consistently, Phe19 is absolutely conserved in all known BlsM and MilB homologs among many bacterial species. When Phe19 was replaced by a tyrosine, a significant reduction in activity (~100-fold) (Table 2) toward CMP and a surprisingly ~two fold increase toward dCMP were observed. This led to drastic alteration in k_{cat}/K_m values for these two substrates, indicating that the substrate specificity of F19Y was reverted to dCMP over the originally preferred substrate, CMP. The mutation of Phe19 to a serine or to an alanine resulted in similar reduction of the enzymatic activity on CMP, suggesting that it is not the chemistry of the side chain but the side chain size that facilitates optimal substrate orientation, favoring the chemical reaction. With a phenylalanine in BlsM, there is enough room in the enzyme active site to accommodate either a CMP or a dCMP to achieve an orientation that is suitable for hydrolysis. Evidently, WT BlsM can hydrolyze both CMP and dCMP. However, the larger rotational freedom of dCMP explains the slightly lower k_{cat}. Based on the crystal structure of MilB in complex with hmCMP (4OHB), the distance between the ζ-carbon of the phenylalanine and the 2′-hydroxyl oxygen of the hmCMP is ~3.7 Å, enough to accommodate only two protons in between. When Phe19 was mutated to a tyrosine, the presence of ζ-OH of the tyrosine limits the available

space for the 2′-OH of a CMP. Potential steric clash between the two hydroxyl groups may disrupt the optimal enzyme and substrate alignment, significantly reducing its hydrolytic activity.[9] dCMP, by lacking the 2′-OH, can instead resume the optimal enzyme-substrate orientation and thus revive the hydrolytic reaction. A slight increase in k_{cat} of F19Y vs. the WT enzyme on dCMP again can be explained by optimal orientation and less rotational freedom imposed by the ζ-OH of the tyrosine. Taken together, we have demonstrated that the amino acid at this position influences the hydrolytic activity by precisely orienting the substrate in the active site through fine-tuning Van der Waals contacts with the substrate.

RCL and NDT preferentially catalyze the hydrolysis of deoxyribonucleotide and deoxynucleoside, respectively.[6,9] Therefore, as expected, a conserved tyrosine residue occupies the equivalent position of Phe19 in BlsM. Consistent with our results, the mutagenesis studies on NDT suggested that the tyrosine residue can help to orient either the substrate at the active site or the side chain of the nucleophilic residue.[21] In addition, our previous kinetic studies on RCL also suggested that Tyr13 contributes to the mechanism of RCL during the slowest kinetic step prior to and including the chemical step but not in substrate binding.[9] Similar mechanisms, with individual amino acid conferring significant substrate selectivity, have also been observed in many other enzyme families. In addition to MilB, the Y-family DNA polymerase, Dpo4[22] also uses a tyrosine (Tyr12) to discriminate dNTP versus NTP. Other similar examples include uridine cytidine kinase, a single-residue mutant (Y93H) of which limits the substrate specificity of the enzyme,[23] and deoxyribonucleoside kinase, the substrate specificity of which changes from pyrimidines to purine on substitution of a few amino acid.[24]

3.4 | Deaminase activity

When Phe19 was mutated to a tyrosine, the hydrolytic activity on CMP was significantly reduced due to suboptimal enzyme-substrate orientation. Surprisingly, F19Y exhibited a noticeable cytidylate deaminase activity. Both TLC migration patterns of the reaction products developed by two different buffer systems and the subsequent MS analysis confirmed the presence of the deamination product UMP. Conceivably, the altered binding mode of CMP in the active site of F19Y, which is caused by the potential steric clash between the ζ-OH of Tyr19 and the 2′-OH of CMP, permits a deamination reaction. Previous study has also shown that both WT BlsM and its Ser98Asp mutant are capable of deaminating cytidine and 2′-deoxycytidine to uridine and deoxyuridine.[1] Similarly, it was suggested that the lack of specific interaction between the highly conserved Ser99 and the 5′-phosphate from nucleoside substrates disrupts proper substrate orientation for hydrolysis, alternatively favoring deamination reaction.[1]

Our results also show that Glu105, the nucleophile in the hydrolysis reaction, was equally important for the alternate deaminase activity of BlsM. All deaminases, including cytidine deaminases,[13] cytosine deaminases,[25] deoxycytidylate deaminases, adenosine,[26] and guanine deaminases,[27,28] are known to contain a catalytically important glutamate residue. This conserved glutamate in the deaminases has been proposed to (a) facilitate the nucleophilic attack by a water molecule that is activated by an enzyme-bound zinc metal ion[29] and (b) help protonate the N4 in cytosine[25] or N1 in purine nucleobases.[26,27] Mutation of Glu63 to an alanine completely abolished deamination capability of APOBEC1 in vitro.[19] The zinc ion in all deaminases is coordinated by either one histidine and two cysteines, or three cysteines that are located in a highly conserved signature zinc binding sequence, **H/C***X*E...**C***XX***C**.[13] BlsM contains only one cysteine, Cys76, apparently lacking the characteristic zinc binding sequence that is commonly shared by all deaminases. Currently, it is not entirely clear whether BlsM is capable of chelating any metal ion near its active site. The fact that BlsM lacks the conserved, characteristic zinc binding motif and that all other homologous hydrolases do not appear to require any metal for catalysis may, arguably, lead the conclusion that BlsM catalyzes deamination reaction in a new metal ion-independent mechanism. However, our studies cannot rule out the possibility of a different metal binding sequence. BlsM structure shows that the side chain of Cys76 protrudes into the active site, in close proximity to the active site residue Glu105. Interestingly, the side chain of one histidine residue, His61, is also pointing into the active site, roughly 3 Å away from the side chain of Cys76 and 5 Å from that of Glu105. In addition, several aspartate and glutamate residues are located nearby, capable of facilitating a potential metal binding in BlsM. Therefore, further investigation on metal binding capability of BlsM will be performed in the future.

In summary, we have provided the solution structure of a nucleotide hydrolase, BlsM. It shares its three-dimensional topology with other members in this recently identified nucleotide hydrolase family, however exhibiting a comparatively smaller active site pocket, possibly contributing to the selection of a pyrimidine nucleobase. Structural and kinetic evidences indicate that Phe19 is the key amino acid that influences the ribose specificity, likely through direct Van der Waals contacts, in providing optimal enzyme-substrate alignment for its

hydrolase activity. Similar to RCL and DRTases, BlsM catalyzes the hydrolysis reaction using a double-displacement mechanism involving a covalent enzyme-substrate intermediate. Finally, although there is no evidence yet supporting the metal ion binding capability of BlsM, this enzyme and its mutant can engage in deaminase activity once the optimal substrate orientation for hydrolysis reaction is altered. Structure comparison with other members in this nucleotide hydrolase family provided insight into the structural and sequence determinants contributing to their rigid substrate specificity. Along with our previous results of RCL, the structural and mechanistic studies of BlsM may help to better understand the biosynthesis pathway of anti-fungal agents and provide rationales for potential structure based inhibitor design for this family of hydrolases.

4 | MATERIALS AND METHODS

4.1 | Overexpression and purification of BlsM

The DNA sequence of BlsM, spanning Gly14-Pro174, was subcloned into pET28b with an N-terminal 6-His tag and a 7-residue linker. Overexpression and purification of BlsM has been detailed previously.[1] For isotopically labeled BlsM, a single colony was taken from an overnight agar plate to inoculate a 5 ml LB medium until it became cloudy, subsequently 500 μl of the LB culture was used to inoculate 25 ml minimal medium and allowed to grow for overnight. This overnight culture was then transferred to 1 l of minimal medium, supplemented with $^{15}NH_4Cl$ and/or ^{13}C-glucose as the sole nitrogen and carbon source, respectively. For fully deuterated BlsM, minimal medium was prepared in 99.8% ^2H_2O (Cambridge Isotope). The incubation temperature was initially kept at 37°C until the cell density reached an OD_{600} of 0.45, at which point the incubation temperature was lowered to 25°C. Protein expression was then induced with 0.1 mM isopropyl β-thiogalactoside when the OD_{600} reached 0.6 and allowed to continue overnight before harvest. Cells from each liter of culture were suspended in 30 ml of cold lysis buffer (50 mM phosphate [pH 8.0], 300 mM NaCl, and 2 mM DTT) and ruptured by French press. The His-tagged BlsM was first purified using a Ni-IDA (GE life science) column, and the elution fractions were further purified by a Superdex-200 gel filtration column (HiLoad 16/60, Amersham Pharmacia) to achieve >95% purity as evidenced by Coomassie-stained SDS-PAGE. The purified enzymes were dialyzed against the final NMR buffer (25 mM sodium phosphate, pH 6.5, 25 mM NaCl, 2 mM DTT, 0.02% NaN_3, and 2 mM BME), concentrated to 0.8–1.2 mM and stored in thin-wall shigemi NMR tubes.

4.2 | NMR experiments and structural calculation

Bruker Avance III HD 800 spectrometer equipped with cryogenic triple-resonance probes with *z*-axis pulsed field gradients were used to collect all data at 308 K. Sequential backbone resonances were assigned using TROSY-based triple resonance experiments, including HNCA, HNCACB, HNCO, HN(CO)CA, and HN(CO)CACB[30] on a $^2H/^{13}C/^{15}N$-triply labeled BlsM. Most of side chain assignments, including all methyl-containing residues, were achieved by 3D HCCH-TOCSY experiment.[31] For stereo-specific assignment of the methyl groups in valine and leucine, J-coupling modulated 2D constant time ^1H-^{13}C HSQC[32] was acquired on a sample that was over-expressed in a media containing both unlabeled and ^{13}C-labeled glucose at a ratio of 9:1.[33] Inter-proton distance restraints were derived from 3D ^{15}N NOESY-TROSY recorded on a ^{15}N-labeled sample, 3D ^{13}C-NOESY-HSQC and modified 3D (^{13}C, ^{13}C)-HMQC-NOESY-HSQC (τ_{mix} 120 ms) on a $^{15}N/^{13}C$-labeled BlsM sample. To unambiguously identify intermolecular interactions, a 3D $^{15}N/^{13}C$ filtered ^{13}C-edited NOESY experiment (τ_{mix} 150 ms)[34] was recorded using a mixture containing equal molar $^{15}N/^{13}C$-labeled and unlabeled BlsM. RDC was measured with ^1H-^{15}N HSQC and TROSY in an interleaved manner[35] using a uniformly ^{15}N-labeled sample that was weakly aligned in the presence of 12% Pf1 phage. All spectra were processed with NMRPipe[36] and analyzed with the aid of NMRView[37] and NMRDraw.[36]

Interproton distance restraints were classified into three categories based on the peak intensities: 1.8–2.7, 1.8–3.5, and 1.8–5.0 Å. Backbone dihedral angles were derived from TALOS+[38] based on the assigned chemical shifts. Structure calculation and refinement were performed using a simulated annealing protocol of XPLOR-NIH[39] in three steps, outlined as follows. First, 200 random structures were allowed to fold in the absence of van der Waals, with fixed force constants for backbone dihedral angles (200 kcal/rad^2) and intra- and intermolecular distance restraints and hydrogen bonds (50 kcal/Å^2), followed by annealing with the temperature decreasing from 1,000 to 300 K while ramping the van der Waals radii from 0 to 0.5 times their regular value, the distance restraints from 0.002 to 50 kcal/Å^2, and the dihedral angle force constant from 200 to 20 kcal/rad^2. Second, the folded structures were refined with fixed van der Waals radii 0.9 times their regular value, again with temperature decreasing from 1,000 to 300 K, while

distance restraints were ramped from 0.05 to 50 kcal/Å^2 and dihedral angle were decreased from 100 to 20 kcal/rad^2. In the final refinement step, RDCs were included, with the force constant being ramped up from 0.0005 to 0.4 kcal/Hz^2 as the annealing temperature decreased from 1,000 to 20 K. Among the 200 were generated, 20 lowest-energy structures were analyzed by using PROCHECK-NMR. Graphics were provided by CHIMERA and MOLMOL program.

4.3 | Site-directed mutagenesis

BlsM mutants were obtained through site-directed mutagenesis using the QuickChange mutagenesis kit (Stratagene). It is noteworthy that at least two nucleotides per codon were changed to minimize potential translational misincorporation. The nucleotide sequence was confirmed by sequencing, and the mutated enzyme was further verified by mass spectrometry. In addition, the WT-like tertiary fold of the mutants was confirmed by ^{1}H NMR. Extra caution was taken to ensure negligible cross-contamination, particularly from trace amount of WT protein. Briefly, a new Ni-column was packed for each mutant, and the size exclusion column was washed extensively according to the manufacturer's recommendations. Protein concentration was measured spectrophotometrically at 280 nm using an extinction coefficient, ε280, of 13,980 M^{-1} cm^{-1}.

4.4 | Kinetics studies of BlsM and its mutants

^{32}P-labeled dCMP and CMP were enzymatically converted from [α-^{32}P]-dCTP and CTP (Perkin-Elmer) using mutT nucleoside triphosphatase from *Escherichia coli*, purified according to the method described by Bhatnagar et al.[40] The monophosphate product was separated by thin-layer chromatography (PEI cellulose, EMD chemicals) using 1 M LiCl as a solvent system and subsequently scraped and extracted with 1 mL of water for 2 hr, followed by lyophilization. The final recovery rate of ^{32}P-dCMP and CMP was ~75%. The rate of hydrolysis of this labeled dCMP was consistent with that of commercial dCMP by a coupled enzymatic assay.[3]

The hydrolytic activity of BlsM was measured in 50 mM Tris pH 7.2 by directly monitoring the liberation of ^{32}P-deoxyribose 5′-monophosphate (dR5P) or ribose 5′-monophosphate (R5P) from the substrate ^{32}P-dCMP or ^{32}P-CMP, respectively. Unless stated otherwise, the standard reaction mixture consisted of variable concentrations of unlabeled substrates with 10,000 cpm of ^{32}P-dCMP or ^{32}P-CMP in a final reaction volume of 60 μl. All reactions were carried out at 37°C. Aliquots of the reaction mixture were collected at various time points, and the reaction were quenched by phenol-chloroform extraction. 4 μl of the resulting sample was spotted on a PEI cellulose TLC plate (EMD Chemicals) and resolved in a solvent system comprising 0.5 M LiCl. The plates were visualized on a Typhoon phosphor imager and quantified using IMAGEQUANT software (GE Health sciences). In all reactions, the steady-state condition was met by allowing <10% on substrate conversion. Initial velocities at each substrate concentration were determined in duplicate datasets and fitted to the Michaelis–Menten equation through nonlinear regression using Kaleida/nospace graph, version 4.03. Control assays, in the absence of enzyme, were routinely included. Any nonenzyme assisted degradation of the substrate was subtracted from the reaction.

4.5 | Deamination activity of F19Y

To identify the deamination product of F19Y, first, an alternative buffer system containing 0.9 M acetic acid and 0.3 M LiCl was used to develop the time-dependent reaction mixture on a PEI cellulose TLC plate as detailed previously by Petersen-Mahrt and Neuberger.[19] Second, for mass spectrometry analysis, 100 μM CMP was incubated with 250 μM F19Y for 4.5 hours at 37 °C. The reaction was quenched by heating to 100 °C for 5 minutes followed by centrifugation to remove the precipitants. The supernatant was desalted by directly loading it onto a Waters Oasis Light SPE column and eluted with 2.8% NH_4OH in methanol and directly injected into a 15 T Solarix FT-ICR using negative polarity electrospray ionization. The identity of each peak was assigned based on the ultra-high resolution of the $[M - H]^-$ peak.

4.6 | Mechanistic studies of BlsM

Methanolysis reaction was performed by incubating 40 μM BlsM with 4 mM substrate in 50 mM sodium phosphate (pH 7.2) in the presence of 20% methanol at 37°C. Aliquots of the reaction mixture at different time points were extracted and quenched by heat denaturation, followed by centrifugation to remove denatured proteins. The supernatant was freeze-dried and the resulting powder was dissolved into 99% ^2H_2O (Cambridge Isotope). The final reaction mixture was analyzed by 1D ^{1}H NMR, and 2D ^{1}H-^{13}C HSQC and HMBC experiments at 800 MHz.

4.7 | Coordinates and resonance assignments

Structural coordinates and list of restraints have been deposited into the RCSB Protein Data Bank (accession number 5VTO). Resonance assignments have been deposited at the RCSB and the Biological Magnetic Resonance Data Bank (accession number 30295).

ACKNOWLEDGMENT

We thank Dr. Bessman, M.J. for providing the mutT clone and Eunjeong Lee for her assistance with the deamination studies. This work was funded in part by National Institutes of Health R21ES024585. We also acknowledge Dr. Somogyi for his assistance with the 15 T Bruker Solarix FT-ICR. The 15 T Bruker SolariXR FT-ICR instrument was supported by NIH Award Number Grant S10 OD018507.

ORCID

Zhengrong Wu https://orcid.org/0000-0002-9402-4622

REFERENCES

1. Grochowski LL, Zabriskie TM. Characterization of BlsM, a nucleotide hydrolase involved in cytosine production for the biosynthesis of blasticidin S. Chembiochem. 2006;7:957–964.
2. Li L, Xu Z, Xu X, et al. The mildiomycin biosynthesis: Initial steps for sequential generation of 5-hydroxymethylcytidine 5′-monophosphate and 5-hydroxymethylcytosine in Streptoverticillium rimofaciens ZJU5119. Chembiochem. 2008;9:1286–1294.
3. Ghiorghi YK, Zeller KI, Dang CV, Kaminski PA. The c-Myc target gene Rcl (C6orf108) encodes a novel enzyme, deoxynucleoside 5′-monophosphate N-glycosidase. J Biol Chem. 2007;282:8150–8156.
4. Versees W, Steyaert J. Catalysis by nucleoside hydrolases. Curr Opin Struct Biol. 2003;13:731–738.
5. Miller RL, Sabourin CL, Krenitsky TA, Berens RL, Marr JJ. Nucleoside hydrolases from Trypanosoma cruzi. J Biol Chem. 1984;259:5073–5077.
6. Armstrong SR, Cook WJ, Short SA, Ealick SE. Crystal structures of nucleoside 2-deoxyribosyltransferase in native and ligand-bound forms reveal architecture of the active site. Structure. 1996;4:97–107.
7. Muzzolini L, Versees W, Tornaghi P, Van Holsbeke E, Steyaert J, Degano M. New insights into the mechanism of nucleoside hydrolases from the crystal structure of the *Escherichia coli* YbeK protein bound to the reaction product. Biochemistry. 2006;45:773–782.
8. Porter DJ, Merrill BM, Short SA. Identification of the active site nucleophile in nucleoside 2-deoxyribosyltransferase as glutamic acid 98. J Biol Chem. 1995;270:15551–15556.
9. Doddapaneni K, Zahurancik W, Haushalter A, Yuan C, Jackman J, Wu Z. RCL hydrolyzes 2′-deoxyribonucleoside 5′-monophosphate via formation of a reaction intermediate. Biochemistry. 2011;50:4712–4719.
10. Doddapaneni K, Mahler B, Pavlovicz R, Haushalter A, Yuan C, Wu Z. Solution structure of RCL, a novel 2′-deoxyribonucleoside 5′-monophosphate N-glycosidase. J Mol Biol. 2009;394:423–434.
11. Yang Y, Padilla A, Zhang C, Labesse G, Kaminski PA. Structural characterization of the mammalian deoxynucleotide N-hydrolase Rcl and its stabilizing interactions with two inhibitors. J Mol Biol. 2009;394:435–447.
12. Sikowitz MD, Cooper LE, Begley TP, Kaminski PA, Ealick SE. Reversal of the substrate specificity of CMP N-glycosidase to Dcmp. Biochemistry. 2013;52:4037–4047.
13. Betts L, Xiang S, Short SA, Wolfenden R, Carter CW Jr. Cytidine deaminase. The 2.3 a crystal structure of an enzyme: Transition-state analog complex. J Mol Biol. 1994;235:635–656.
14. Zhao G, Wu G, Zhang Y, et al. Structure of the N-glycosidase MilB in complex with hydroxymethyl CMP reveals its Arg23 specifically recognizes the substrate and controls its entry. Nucleic Acids Res. 2014;42:8115–8124.
15. Kline PC, Serianni AS. C-13-enriched ribonucleosides synthesis and application of C-13-H-1 and C13-C13 spin-coupling constants to assess furanose and n-glycoside bond conformation. J Am Chem Soc. 1990;112:7373–7381.
16. Parkin DW, Horenstein BA, Abdulah DR, Estupinan B, Schramm VL. Nucleoside hydrolase from Crithidia fasciculata. Metabolic role, purification, specificity, and kinetic mechanism. J Biol Chem. 1991;266:20658–20665.
17. Shallom D, Belakhov V, Solomon D, Shoham G, Baasov T, Shoham Y. Detailed kinetic analysis and identification of the nucleophile in alpha-L-arabinofuranosidase from Geobacillus stearothermophilus T-6, a family 51 glycoside hydrolase. J Biol Chem. 2002;277:43667–43673.
18. McCarter JD, Withers SG. Mechanisms of enzymatic glycoside hydrolysis. Curr Opin Struct Biol. 1994;4:885–892.
19. Petersen-Mahrt SK, Neuberger MS. In vitro deamination of cytosine to uracil in single-stranded DNA by apolipoprotein B editing complex catalytic subunit 1 (APOBEC1). J Biol Chem. 2003;278:19583–19586.
20. Pitson SM, Voragen AG, Beldman G. Stereochemical course of hydrolysis catalyzed by arabinofuranosyl hydrolases. FEBS Lett. 1996;398:7–11.
21. Short SA, Armstrong SR, Ealick SE, Porter DJ. Active site amino acids that participate in the catalytic mechanism of nucleoside 2′-deoxyribosyltransferase. J Biol Chem. 1996;271:4978–4987.
22. Sherrer SM, Beyer DC, Xia CX, Fowler JD, Suo Z. Kinetic basis of sugar selection by a Y-family DNA polymerase from Sulfolobus solfataricus P2. Biochemistry. 2010;49:10179–10186.
23. Tomoike F, Nakagawa N, Kuramitsu S, Masui R. A single amino acid limits the substrate specificity of Thermus thermophilus uridine-cytidine kinase to cytidine. Biochemistry. 2011;50:4597–4607.
24. Knecht W, Sandrini MP, Johansson K, Eklund H, Munch-Petersen B, Piskur J. A few amino acid substitutions can convert deoxyribonucleoside kinase specificity from pyrimidines to purines. EMBO J. 2002;21:1873–1880.
25. Ko TP, Lin JJ, Hu CY, Hsu YH, Wang AH, Liaw SH. Crystal structure of yeast cytosine deaminase insights into enzyme mechanism and evolution. J Biol Chem. 2003;278:19111–19117.
26. Losey HC, Ruthenburg AJ, Verdine GL. Crystal structure of *Staphylococcus aureus* tRNA adenosine deaminase TadA in complex with RNA. Nat Struct Mol Biol. 2006;13:153–159.

27. Bitra A, Biswas A, Anand R. Structural basis of the substrate specificity of cytidine deaminase superfamily guanine deaminase. Biochemistry. 2013;52:8106–8114.
28. Bitra A, Hussain B, Tanwar AS, Anand R. Identification of function and mechanistic insights of guanine deaminase from *Nitrosomonas europaea*: Role of the C-terminal loop in catalysis. Biochemistry. 2013;52:3512–3522.
29. Snider MJ, Reinhardt L, Wolfenden R, Cleland WW. 15N kinetic isotope effects on uncatalyzed and enzymatic deamination of cytidine. Biochemistry. 2002;41:415–421.
30. Grzesiek S, Dobeli H, Gentz R, Garotta G, Labhardt AM, Bax A. ^{1}H, ^{13}C, and ^{15}N NMR backbone assignments and secondary structure of human interferon. Biochemistry. 1992;31:8180–8190.
31. Bax A, Grzesiek S. Methodological advances in protein NMR. Acc Chem Res. 1993;26:131–138.
32. Vuister GW, Bax A. Resolution enhancement and spectral editing of uniformly ^{13}C-enriched proteins by homonuclear broadband ^{13}C decoupling. J Magn Reson. 1992;98:428–435.
33. Neri D, Szyperski T, Otting G, Senn H, Wuthrich K. Stereospecific nuclear magnetic resonance assignments of the methyl groups of valine and leucine in the DNA-binding domain of the 434 repressor by biosynthetically directed fractional ^{13}C labeling. Biochemistry. 1989;28:7510–7516.
34. Lee W, Revington MJ, Arrowsmith C, Kay LE. A pulsed field gradient isotope-filtered 3D ^{13}C HMQC-NOESY experiment for extracting intermolecular NOE contacts in molecular complexes. FEBS Lett. 1994;350:87–90.
35. Weigelt J. Single scan, sensitivity-and gradient-enhanced TROSY for multidimensional NMR experiments. J Am Chem Soc. 1998;120:10778–10779.
36. Delaglio F, Grzesiek S, Vuister GW, Zhu G, Pfeifer J, Bax A. Nmrpipe—A multidimensional spectral processing system based on Unix pipes. J Biomol NMR. 1995;6:277–293.
37. Johnson BA, Blevins RA. NMRView: A computer program for the visualization and analysis of NMR data. J Biomol NMR. 1994;4:603–614.
38. Cornilescu G, Delaglio F, Bax A. Protein backbone angle restraints from searching a database for chemical shift and sequence homology. J Biomol NMR. 1999;13:289–302.
39. Schwieters C, Kuszewski J, Tjandra N, Clore G. The Xplor-NIH NMR molecular structure determinsation package. J Magn Reson. 2003;160:65–73.
40. Bhatnagar SK, Bullions LC, Bessman MJ. Characterization of the mutT nucleoside triphosphatase of *Escherichia coli*. J Biol Chem. 1991;266:9050–9054.

How to cite this article: Kang M, Doddapaneni K, Sarni S, Heppner Z, Wysocki V, Wu Z. Solution structure of the nucleotide hydrolase BlsM: Implication of its substrate specificity. *Protein Science*. 2020;29:1760–1773. https://doi.org/10.1002/pro.3812